

SITULA EMT09-554.665 – TIN BRONZE – IRON AGE – SWITZERLAND

Artefact name	Situla EMT09-554.665
Authors	Christian. Degrigny (HE-Arc CR, Neuchâtel, Neuchâtel, Switzerland) & Marie-Jeanne. Scholl (HE-Arc CR, Neuchâtel, Neuchâtel, Switzerland) & Valentin. Boissonnas (HE-Arc CR, Neuchâtel, Neuchâtel, Switzerland)
Url	/artefacts/538/

✧ The object



Fig. 1: Situla (Archeodunum (Gollion), 2009) inverted as found in situ,

Credit HE-Arc CR, M-J.Scholl.

✧ Description and visual observation

Description of the artefact	Situla (Fig. 1). Attached to two riveted iron loops is an iron handle terminating in two swan heads (not shown here). Dimensions of the main body: Hmax = 340mm, Ømax = 220mm.
Type of artefact	Situla
Origin	Mormont sanctuary, La Sarraz, Vaud, Switzerland
Recovering date	Excavated in 2011
Chronology category	Iron Age
chronology tpq	<input type="text" value="140"/> B.C. ▾
chronology taq	<input type="text" value="30"/> B.C. ▾
Chronology comment	La Tène D
Burial conditions / environment	Soil
Artefact location	Musée cantonal d'archéologie et d'histoire, Lausanne, Vaud
Owner	Musée cantonal d'archéologie et d'histoire, Lausanne, Vaud
Inv. number	EMT09/554.665

Complementary information

The size and quality of the object makes it likely that it was reserved for important occasions or for ritual use. Secondary use could be a votive offering. Burial condition: inside a 3 meters deep hole in upside-down position.

Study area(s)



Credit HE-Arc CR, M-J.Scholl.

Fig. 2: Location of sampling area and sample selected from detached fragments,

Binocular observation and representation of the corrosion structure

The schematic representation below gives an overview of the corrosion layers encountered on the situla from a first visual macroscopic observation (additional e and i within the coding correspond to strata in contact with the environment (e) and internal strata (i)).

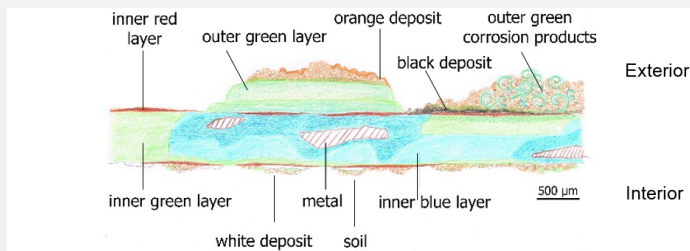
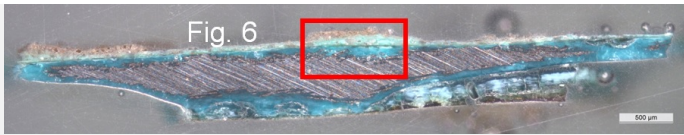


Fig. 3: Stratigraphic representation of the situla in cross-section by macroscopic observation,

S: soil (sediment)
D1: black deposit
D2: orange deposit
D3: white deposit
CP1e: outer green corrosion products (might be curly)
CP2i: inner red layer
CP3i: outer green layer
CP4i: inner green layer
CP5i: inner blue layer
M: metal
 Credit HE-Arc CR, M-J.Scholl.

MiCorr stratigraphy(ies) – Bi

Sample(s)



Credit HE-Arc CR, M-J.Scholl.

Fig. 4: Micrograph of the cross-section of the sample taken from the detached fragment of the situla showing the location of Fig. 6. Unetched, dark field, 50x,

Description of sample	The sample was cut from a detached fragment of the upper part of the main body of the situla in Fig. 2. The cross-section is representative of the entire thickness (0.5 mm) of the object's body where on the outside there is a thicker accumulation of corrosion including curly malachite clusters (Fig. 3). A metallic core is still present inside the corrosion products layers (Fig. 4).
Alloy	Tin Bronze
Technology	Cold worked (hammering on a counter-mould), annealed but no final annealing
Lab number of sample	None
Sample location	HE-Arc CR, Neuchâtel, Neuchâtel
Responsible institution	Musée cantonal d'archéologie et d'histoire, Lausanne, Vaud
Date and aim of sampling	2014, metallography and chemical analyses (FTIR, SEM-EDS)

Complementary information

Nothing to report.

∨ Analyses and results

Analyses performed:

Metallography (etched with ferric chloride reagent), SEM-EDS, FTIR, Raman spectroscopy and XRD.

∨ Non invasive analysis

∨ Metal

The remaining metal is a dense tin bronze (Fig. 7, Table 1), showing no inclusion. In bright field, the etched alloy shows a structure principally consisting of polygonal alpha phase grains (Fig. 8). Some of the grains include twin lines (Fig. 9). The presence of strain lines (slip lines) indicates a final cold work without annealing (Fig. 9).

Elements	Cu	Sn
mass%	90	10

Table 1: Chemical composition of the metal. Method of analysis: SEM-EDS, Lab of Electronic Microscopy and Microanalysis, IMA (Néode), HEI Arc.

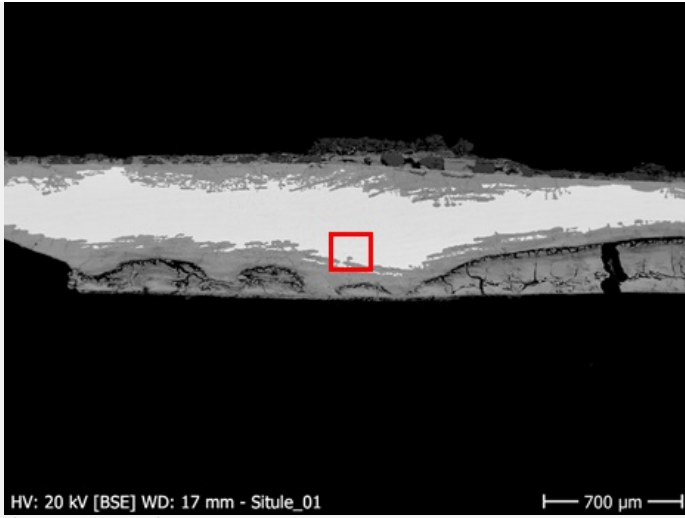


Fig. 7: SEM image, BSE-mode, of the metal sample from Fig. 4. Area of Fig. 8 is marked by a red square,

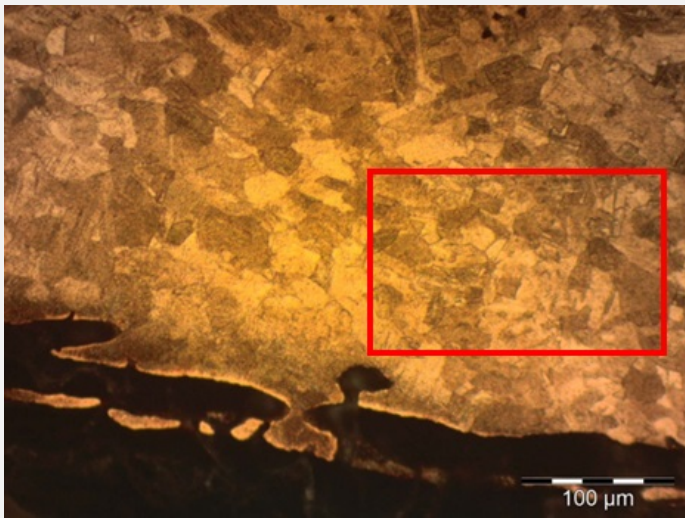


Fig. 8: Micrograph of the etched metal structure from Fig. 7 (detail), etched, bright field, 50x. The alpha phase of the alloy shows polygonal grains. Area of Fig. 9 is marked by a red rectangle,



Fig. 9: Micrograph of the selected area of Fig. 8, etched, bright field, 500x. The grains show both twin and strain lines,

Microstructure	Polygonal grain with twin and strain lines
First metal element	Cu
Other metal elements	Sn

Complementary information

Nothing to report.

Corrosion layers

The corrosion crust is heterogeneous and has in places completely replaced the metal. The metal – corrosion products interface is irregular due to transgranular corrosion (Figs 7-8). In most cases, the corrosion crust can be divided in three main layers: an inner compact blue layer directly on the metal core (CP5, Figs. 6, 10 and 11 and CP3, Fig. 5). In areas of extensive corrosion this blue layer coexists with a friable green layer (CP4, Figs. 6, 10 and 11 and CP2, Fig. 5). Depending on the area either a very fine dark green (CP3, Fig. 6 and Fig. 10) or red corrosion layer (CP2, Fig. 6 and Fig. 10) marks the limit of the original surface. It is followed by an external fourth layer, consisting of friable and sometimes curly pale green corrosion products intermingled with soil products (CP1, Fig. 6 and Fig. 10 and 13). In heavily worked and fragile parts of the object a cleavage between the inner layers of blue and green corrosion is present, rendering the green corrosion vulnerable to loss (Fig. 11).

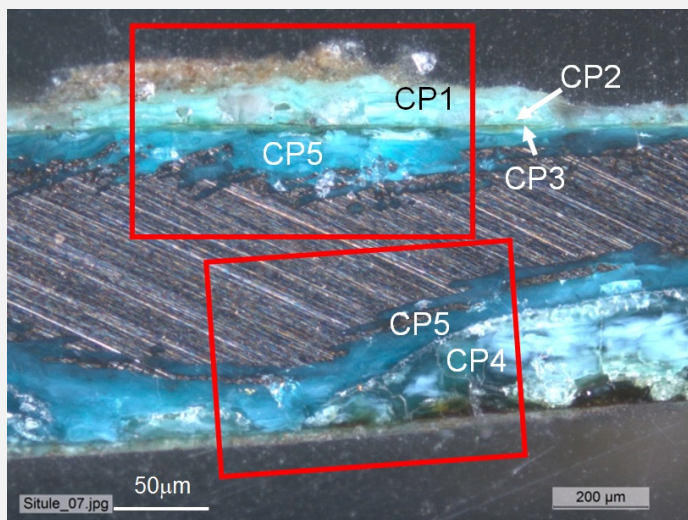
There are 2 stratigraphies (Fig. 5 corresponding to the interior face of the situla and Fig. 6 to its exterior face). The strata are similar in composition but their coding is different: CP1 to CP3 in Fig. 5 correspond to CP3 to CP5 in Fig. 6. Since the stratigraphy of Fig. 6 is more complete, the composition of each of its strata is given below.

The inner layers (CP3-CP5) are Sn and O-rich and depleted in Cu (Table 2). The outer layers (CP1 and CP2) are Cu and O-rich, contain no Sn, and are contaminated with Ca, Si, Al and Fe coming from the soil (Fig. 12). The colour of the corrosion crust varies according to the content of Sn (the more Sn, the darker green or blue the corrosion). FTIR on the inner blue (CP5 and Fig. 14) and outer green (CP1 and Fig. 15) layers were difficult to interpret. Only malachite could be identified in both cases. XRD spectra could not be interpreted because of the deficiency of peaks.

The limit of the original surface is well defined (interface of CP1 and CP2) but due to the fragility of the inner corrosion layers it was difficult to uncover.

Elements	O	Cu	Sn
Outer green layer (CP1)	+++	+++	nd
Inner green layer (CP4)	++	+	+++
Inner blue layer (CP5)	++	+	+++
Remnant metal phase	nd	+++	+

Table 2: Chemical composition of the corrosion crust from Fig. 10. SEM-EDS, Lab of Electronic Microscopy and Microanalysis, IMA (Néode) (+++: high concentration, ++ medium concentration, + low concentration, nd: not-detected).



Credit HE-Arc CR.

Fig. 10: Micrograph of the metal sample from Fig. 4, unetched, dark field, 50x. Areas of Fig. 11 (bottom, corresponding to the stratigraphy of Fig. 5) and Figs. 12 and 13 (top, corresponding to the stratigraphy of Fig. 6) are marked by a rectangle. Codes are those of Fig. 6.

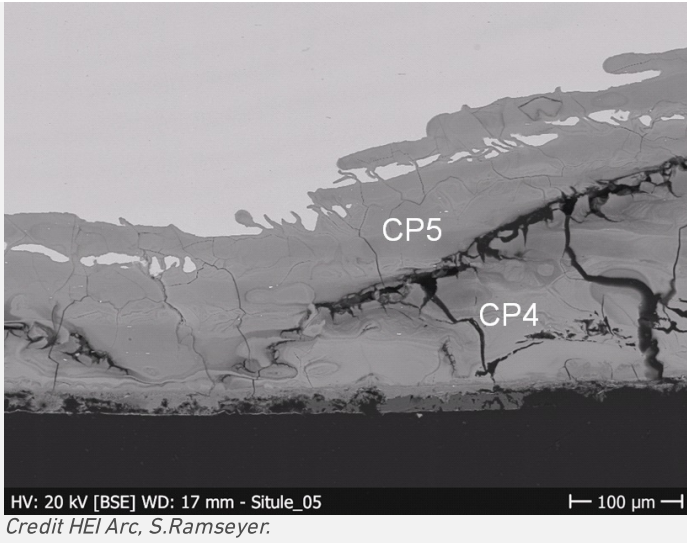


Fig. 11: SEM image, BSE-mode of the metal sample from Fig. 10 (detail) showing cleavage between the inner blue (CP5) and green (CP4) layers of Fig. 6,

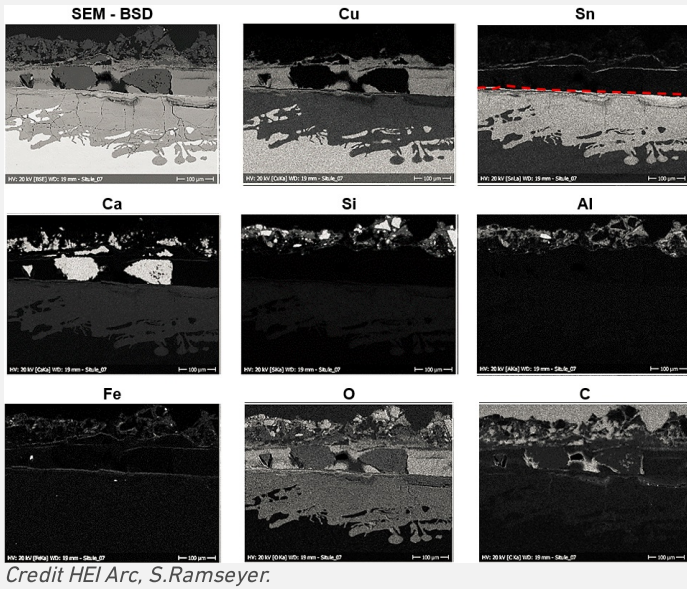


Fig. 12: SEM image, SE-mode, and elemental chemical distribution of the selected area of Fig. 10. In red: the limit of the original surface highlighted by the enriched tin layer. Method of examination: SEM-EDS, Lab of Electronic Microscopy and Microanalysis, IMA (Néode), HEI Arc,

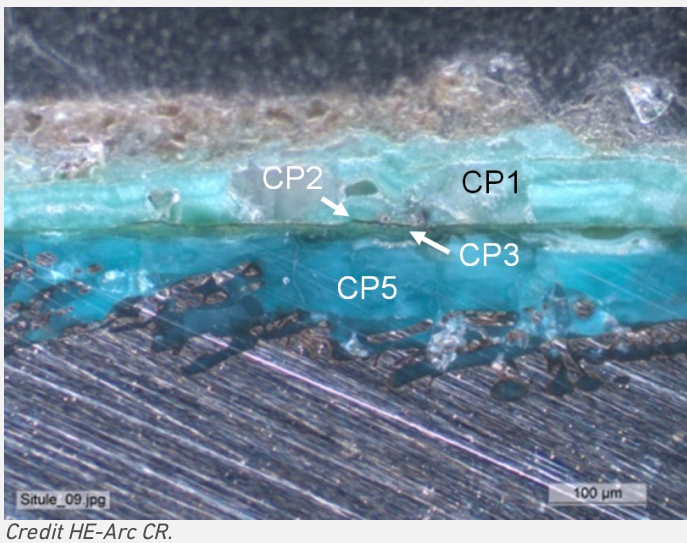
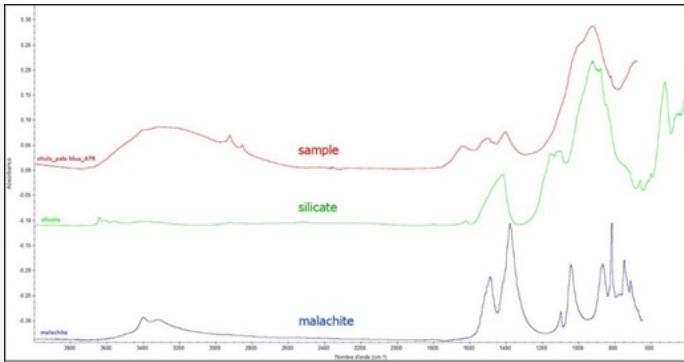
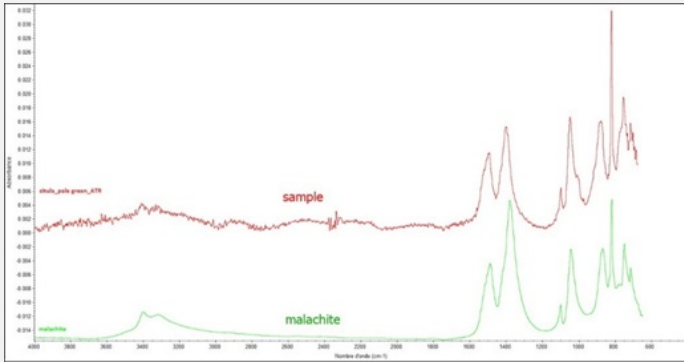


Fig. 13: Micrograph of the metal / corrosion interface (detail of Fig. 10) unetched, dark field, 100x. The outer layer (CP1 of Fig. 6) incorporates soil material and the thin dark layer (CP2 of Fig. 6) highlights the limit of the original surface,



Credit HE-Arc CR.

Fig. 14: FTIR spectrum (ATR mode) of the inner blue layer compared to the silicate and malachite standard spectrum. Method of analysis: FTIR spectroscopy, HE- Arc CR,



Credit HE-Arc CR.

Fig. 15: FTIR spectrum (ATR mode) of the outer green layer compared to the malachite standard spectrum. Method of analysis: FTIR spectroscopy, HE-Arc CR.,

Corrosion form	Multiform - transgranular
Corrosion type	Type I (Robbiola)

Complementary information

Nothing to report.

∨ MiCorr stratigraphy(ies) – CS

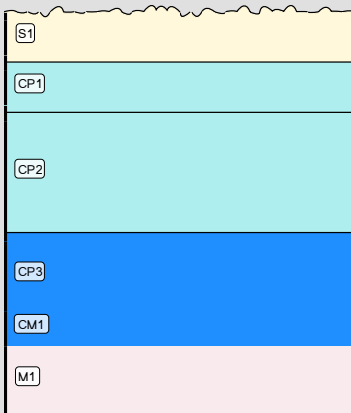


Fig. 5: Stratigraphic representation of the sample taken from the detached fragment of the situla in cross-section using the MiCorr application. The characteristics of the strata are only accessible by clicking on the drawing that redirects you to the search tool by stratigraphy representation. This representation shows the exterior face and can be compared to Fig. 10 (bottom red rectangle), Credit HE-Arc CR, M-J.Scholl.



Fig. 6: Stratigraphic representation of the sample taken from the detached fragment of the situla in cross-section using the MiCorr application. The characteristics of the strata are only accessible by clicking on the drawing that redirects you to the search tool by stratigraphy representation. This representation shows the interior face and can be compared to Fig. 10 (top red rectangle), Credit HE-Arc CR, M-J.Scholl.

✧ Synthesis of the binocular / cross-section examination of the corrosion structure

The schematic representation of corrosion layers of Fig. 3 integrating additional information (e and i within the coding correspond to strata in contact with the environment (e) and internal strata (i)) based on the analyses carried out is given in Fig. 16.

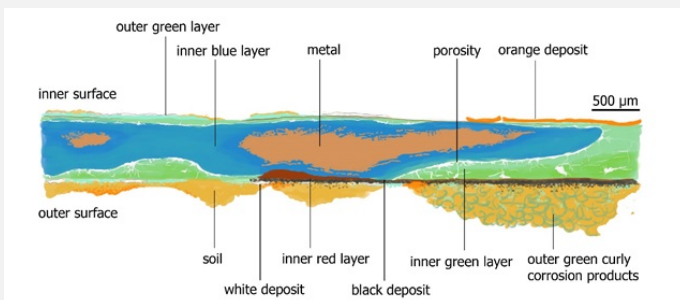


Fig. 16: Improved stratigraphic representation of the situla from visual observations and analyses,

Strata	Composition
Soil (S)	Ca, Si, Al, Fe
Black deposit (D1)	C
Orange deposit (D2)	Ferrous oxides
White deposit (D3)	Ca
Outer green curly corrosion product (CP1e)	Copper carbonates (curly malachite)
Inner red (CP2i)	Copper oxide (cuprite ?)
Outer green layer (CP3i)	Copper carbonates (malachite)
Inner green layer (CP4i)	Copper carbonates (?) + Sn
Inner blue layer (CP5i)	Copper carbonates (?) + Sn
Remnant metal phase (M)	Bronze (90%Cu, 10% Sn)

Credit HE-Arc CR, M-J.Scholl.

✧ Conclusion

The metal structure of this low-tin bronze shows extensive cold work and multiple annealing cycles with a final cold work. The total absence of inclusions highlights a highly developed knowledge in bronze metallurgy. The metal is much corroded. Transgranular corrosion is visible. The majority of the internal corrosion products are composed of copper carbonates that have replaced much of the metal. Curly malachite has developed in clusters on the outside of the surface. This pattern is characteristic of a long-term burial period. The presence of inner enriched Sn layers shows a decuprification phenomenon (dissolution of Cu). Because of the friable nature of the inner green layer that supports the limit of the original surface, as well as its cleavage with the blue layer underneath, the original surface has become very fragile. The corrosion is thought to be of type 1 according to Robbiola et al. 1998.

✧ References

References on object and sample

Reference object

1. Archeodunum (Gollion) (2009) Le Mormont : un sanctuaire des Helvètes en terre vaudoise vers 100 avant J.-C. Section de l'archéologie cantonale, Lausanne.

Reference sample

2. Scholl, M.-J. (2013) Situle en bronze et anse en fer, EMT09/554.665, vers 100 av. J.-C., La Sarraz/Eclépens, Le Mormont (VD), Musée cantonal d'archéologie et d'histoire, Lausanne. Rapport d'intervention, Haute Ecole Arc de Conservation-restauration, Neuchâtel [not published].

3. Eggert, G. (2007) Pseudomorph or corrosion? The enigma of the curly malachite, in Metal07 - Proceedings of the International Conference on Metals Conservation, Degryny, C., Van Langh, R., Ankersmit, B. and Joosten, I. (eds), Rijksmuseum, Amsterdam, 1, 57-60.

References on analytic methods and interpretation

4. Robbiola, L., Blengino, J.-M., Fiaud, C. (1998) Morphology and mechanisms of formation of natural patinas on archaeological Cu-Sn alloys, Corrosion Science, 40, 12, 2083-2111.